

# Characterization of the catalytic flexible loop in the dihydroorotase domain of the human multi-enzymatic protein CAD

Received for publication, August 23, 2018, and in revised form, October 8, 2018. Published, Papers in Press, October 12, 2018, DOI 10.1074/jbc.RA118.005494

 Francisco del Caño-Ochoa<sup>‡1,2</sup>,  Araceli Grande-García<sup>§1</sup>, María Reverte-López<sup>‡</sup>, Marco D'Abramo<sup>¶</sup>, and  Santiago Ramón-Maiques<sup>‡3</sup>

From the <sup>‡</sup>Department of Genome Dynamics and Function, Centro de Biología Molecular Severo Ochoa (CSIC-UAM), Madrid 28049, Spain, the <sup>§</sup>Structural Biology Programme, Spanish National Cancer Research Centre (CNIO), Madrid 28029, Spain, and the <sup>¶</sup>Department of Chemistry, Sapienza University of Rome, Rome 00185, Italy

Edited by Norma M. Allewell

The dihydroorotase (DHOase) domain of the multifunctional protein carbamoyl-phosphate synthetase 2, aspartate transcarbamoylase, and dihydroorotase (CAD) catalyzes the third step in the *de novo* biosynthesis of pyrimidine nucleotides in animals. The crystal structure of the DHOase domain of human CAD (huDHOase) revealed that, despite evolutionary divergence, its active site components are highly conserved with those in bacterial DHOases, encoded as monofunctional enzymes. An important element for catalysis, conserved from *Escherichia coli* to humans, is a flexible loop that closes as a lid over the active site. Here, we combined mutagenic, structural, biochemical, and molecular dynamics analyses to characterize the function of the flexible loop in the activity of CAD's DHOase domain. A huDHOase chimera bearing the *E. coli* DHOase flexible loop was inactive, suggesting the presence of distinctive elements in the flexible loop of huDHOase that cannot be replaced by the bacterial sequence. We pinpointed Phe-1563, a residue absolutely conserved at the tip of the flexible loop in CAD's DHOase domain, as a critical element for the conformational equilibrium between the two catalytic states of the protein. Substitutions of Phe-1563 with Ala, Leu, or Thr prevented the closure of the flexible loop and inactivated the protein, whereas substitution with Tyr enhanced the interactions of the loop in the closed position and reduced fluctuations and the reaction rate. Our results confirm the importance of the flexible loop in CAD's DHOase domain and explain the key role of Phe-1563 in configuring the active site and in promoting substrate strain and catalysis.

Dihydroorotase (DHOase)<sup>4</sup> (EC 3.5.2.3) is a ubiquitous Zn metalloenzyme that catalyzes the reversible condensation of carbamoyl aspartate (CA-asp) to dihydroorotate (DHO) in the third step of the *de novo* biosynthesis of pyrimidine nucleotides (1). Despite being present in all organisms, there is an intriguing number of different DHOase forms (2, 3). Understanding the differences among DHOases, particularly in the layout of the active site, could lead to the development of improved inhibitors for treating microbial and parasitic infections or as anti-inflammatory or antitumoral agents (4–8).

In animals, DHOase is fused with carbamoyl-phosphate synthetase and aspartate transcarbamoylase (ATCase), the enzymes that catalyze the previous steps in the *de novo* pathway, forming a single polypeptide of ~250 kDa named CAD that self-assembles into hexameric particles (9, 10) (reviewed in Refs. 1 and 11). On the contrary, in bacteria, DHOases are encoded as separated proteins that function independently (bacterial type II DHOases, e.g. *Escherichia coli*) or in association with ATCase (bacterial type I, e.g. *Aquifex aeolicus*). The evolutionary advantages for the fusion of DHOase into the multi-enzymatic CAD protein, as well as the catalytic and regulatory mechanisms of such a large complex, are yet to be uncovered. To this end, detailed information about the structures of the individual enzymatic domains and about the architecture of CAD are needed.

Previously, we reported the crystal structure of the DHOase domain of human CAD (huDHOase) (2, 12). huDHOase is a dimer with each subunit folding in a  $(\beta/\alpha)_8$ -barrel motif, holding an active site nucleated by two  $\text{Zn}^{2+}$  ions, and shaped by the loops connecting the carboxyl edge of the central  $\beta$ -barrel with the outer  $\alpha$ -helices (Fig. 1A). The structure proves that, despite the existence of specific peripheral structural motifs and distinctive quaternary organizations, there is a high conservation of the active site elements between eukaryotic and prokaryotic DHOases (2, 13–15).

One important element proven to be conserved from *E. coli* to humans is a loop that fluctuates between a closed (loop-in) or open

This work was supported by the Spanish Ministry of Science, Innovation and Universities (BFU2016-80570-R; AEI/FEDER, UE), by the European Community's Seventh Framework Programme (FP7/2007-2013) under BioStruct-X (Grant 283570) and by the Spanish National Cancer Research Centre (CNIO) Intramural Programme. The authors declare that they have no conflicts of interest with the contents of this article.

This article contains Figs. S1–S4 and Tables S1 and S2.

The atomic coordinates and structure factors (codes 6HG1, 6HG2, 6HG3, 6HFI, 6HFE, 6HFD, 6HFF, 6HFH, 6HFP, 6HFL, 6HFR, 6HFJ, 6HFQ, 6HFK, 6HFN, 6HFS, and 6HFU) have been deposited in the Protein Data Bank (<http://www.pdb.org/>).

<sup>1</sup> Both authors contributed equally to this work.

<sup>2</sup> A fellow of the Severo Ochoa Excellence Program.

<sup>3</sup> To whom correspondence should be addressed. Tel.: 34-91 1964698; E-mail: [santiago.ramon@cbm.csic.es](mailto:santiago.ramon@cbm.csic.es).

<sup>4</sup> The abbreviations used are: DHOase, dihydroorotase; DHO, dihydroorotate; huDHOase, human dihydroorotase; ecDHOase, *Escherichia coli* dihydroorotase; CA-asp, carbamoyl aspartate; CAD, carbamoyl-phosphate synthetase 2, aspartate transcarbamoylase, and dihydroorotase; FOA, fluoroorotic acid; MD, molecular dynamics; SEC-MALS, size-exclusion chromatography multi-angle light scattering; EFL, *E. coli* flexible loop (mutant); ATCase, aspartate transcarbamoylase; His<sub>6</sub>-MBP, His<sub>6</sub>-tagged maltose-binding protein.

This is an Open Access article under the CC BY license.

## A catalytic flexible loop in the DHOase domain of human CAD

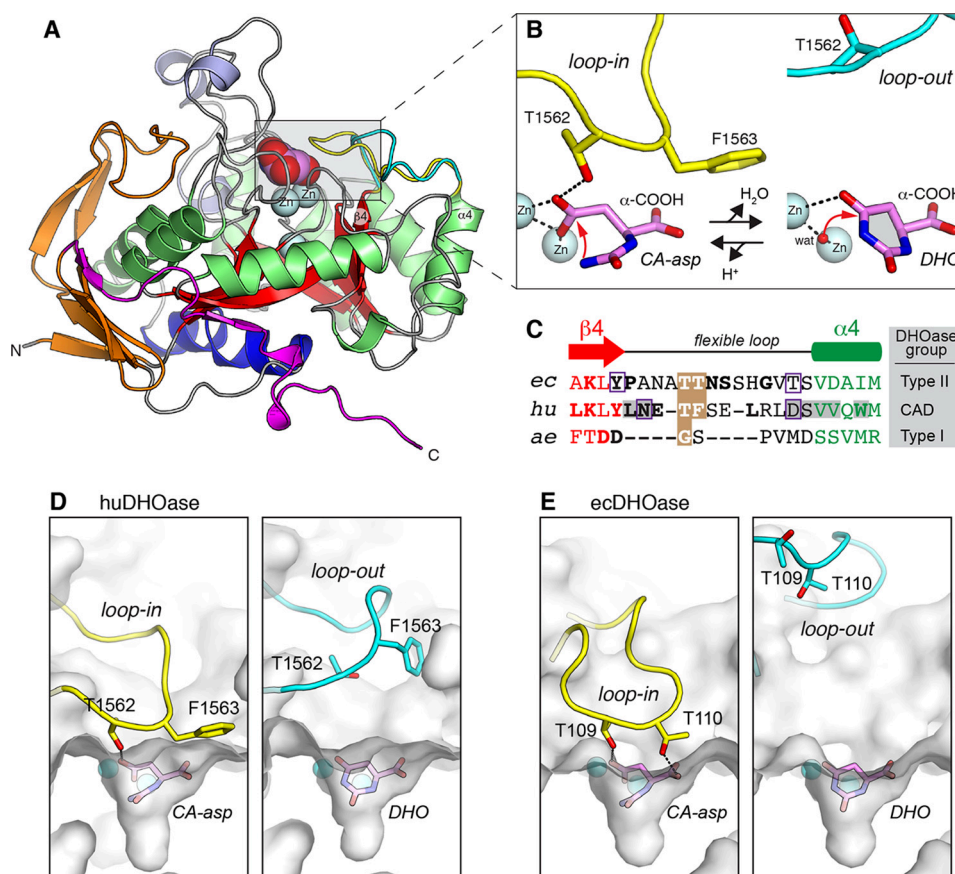


**Figure 1.** A, crystal structure of huDHOase bound to DHO (PDB ID: 4C6L). The central  $\beta$ -barrel is shown in red, and  $\text{Zn}^{2+}$  ions are shown as cyan spheres. The flexible loop is represented in closed (yellow) and open (cyan) conformations. B, ball-and-stick representation of the reversible reaction, showing the position of the  $\text{Zn}^{2+}$  ions, the attacking water (wat), and the flexible loop. Red arrows indicate a nucleophilic attack. C, sequence alignment of the flexible loop region in the DHOases from *E. coli* (ec; bacterial type II), human (hu; domain within multifunctional CAD), and *A. aeolicus* (ae; bacterial type I). Residues are colored according to the secondary structure, which is shown above the alignment. Residues in bold are highly conserved ( $\geq 90\%$  identity) within their respective groups. Distinctive signatures are highlighted on a brown background, and huDHOase residues that change their accessibility upon dimerization are shown on a gray background. Hinge residues are indicated by a purple box. D and E, comparison of the open and closed conformations of the flexible loop in human (D) and *E. coli* (E) DHOases. The active site is represented on a semitransparent surface with  $\text{Zn}^{2+}$  ions as cyan spheres. Dashed lines represent hydrogen bonds.

(loop-out) position whether CA-asp or DHO are bound, respectively, to the active site (Fig. 1, A and B) (2, 16, 17). This flexible loop reaches in toward the active site with CA-asp bound and is proposed to aid in catalysis by orienting and increasing the electrophilicity of the substrate, excluding water molecules, and stabilizing the transition-state (16–18). Then, upon the formation of DHO, the loop moves away from the active site, facilitating product release. As an exception, bacterial type I DHOases present a rigid and shorter loop that interacts minimally with the substrate (19) (Fig. 1C), requiring the intimate association with ATCase to complete the active site and attain full activity (19–21).

The flexible loop exhibits a two-amino acid signature that is characteristic for each DHOase type (2, 15, 18) (Fig. 1C). In all cases, the first residue is a threonine, namely Thr-109 in *E. coli* DHOase (ecDHOase) or Thr-1562 in huDHOase, which interacts through its side chain with the  $\beta$ -COOH group of CA-asp (Fig. 1, B–E). In *E. coli* and other bacterial type II DHOase, the second specific residue is also a Thr (Thr-110 in ecDHOase) that occupies the tip of the loop and binds through its side chain to the  $\alpha$ -COOH group of CA-asp (Fig. 1, C and E). Mutating either of the two Thr inactivates ecDHOase, proving the importance of the loop in the reaction (16). In CAD, on the other hand, the flexible loop is two residues shorter than in ecD-

HOase and replaces the second Thr by a conserved Phe (Phe-1563 in huDHOase) (Fig. 1, C and D) (2). We demonstrated previously that mutations T1562A or F1563A impair the activity of huDHOase (2) proving that, as in ecDHOase, the flexible loop also plays a key functional role in CAD.

Now, we further interrogated how the flexible loop contributes to the activity of huDHOase. We report that a human DHOase chimera bearing the flexible loop of *E. coli* DHOase is inactive, suggesting that, despite having a conserved function, the flexible loops might have different functional and structural features. We also produced four different huDHOase variants, replacing Phe-1563 at the tip of the flexible loop with Ala, Thr, Leu, or Tyr, measured the activities, and determined their crystal structures. These results, combined with molecular dynamics simulations, highlight the key contribution of the phenylalanine in configuring the active site of CAD's DHOase domain.

## Results

### A human DHOase chimera with the flexible loop of *E. coli* DHOase is inactive

To test the functional similarity between the flexible loops of human and *E. coli* DHOases, we replaced the loop of huD-

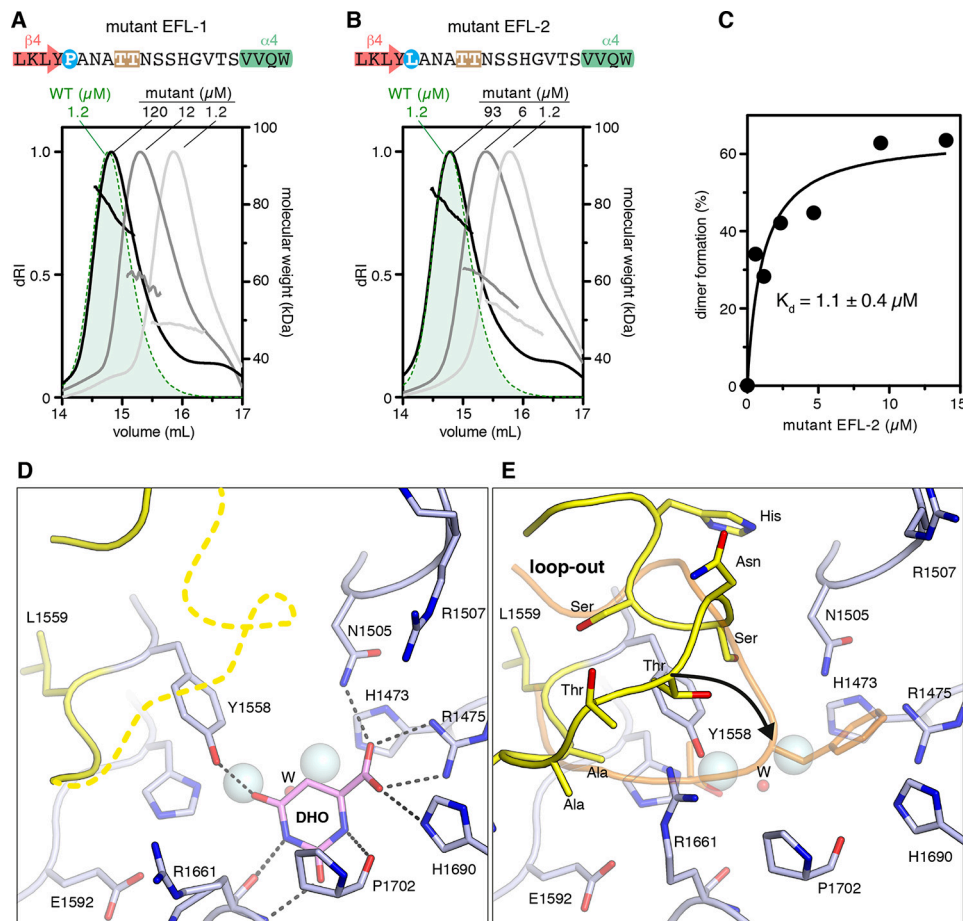


**Figure 2.** A and B, SEC-MALS analysis of EFL-1 (A) and EFL-2 (B) mutants. The mutated region is shown above the graphs and is colored as described for Fig. 1C. The different residue at the beginning of the loop is shown on a cyan background. The elution profiles and molecular weight measurements of the mutants are shown in black, gray, and light gray, corresponding to decreasing protein concentrations, whereas WT is shown in green. C, sedimentation velocity experiment of EFL-2. D, cartoon representation of the active site of mutant EFL-2 bound to DHO. The  $\text{Zn}^{2+}$  atoms and the bridging water are shown as cyan and red spheres, respectively. Dashed lines represent electrostatic interactions. The flexible loop is colored in yellow, and nontraceable regions are indicated with a thick dashed line. E, EFL-2 apostructure. The loop of huDHOase WT in closed conformation and the side chain of Phe-1563 are shown in orange as a reference. A black arrow indicates the movement that the loop should undergo to reach the closed state.

HOase ( $^{1559}\text{LNETFSELRLD}^{1569}$ ) with the equivalent region in ecDHOase ( $^{105}\text{PANATTNSSHGVT}^{117}$ ) (Fig. 1C). We generated two huDHOase chimeras, one with the exact *E. coli* flexible loop (hereafter referred to as mutant EFL-1) and another one that preserves residue Leu-1559 at the beginning of the loop (mutant EFL-2) in case a proline could affect the movements of the hinge residues after strand  $\beta_4$  (Figs. 1C and 2, A and B). Both mutants were produced following a protocol similar to that for huDHOase wildtype (WT) (Fig. S1), although the lower yield suggested folding or solubility problems. Indeed, salt concentration in final size-exclusion chromatography (SEC) was increased (from 0.15 to 0.25 M) to prevent protein precipitation.

Analysis by SEC coupled to multi-angle light scattering (SEC-MALS) showed that the EFL mutants injected at  $1.2\ \mu\text{M}$  eluted in a main peak corresponding to a monomer, whereas the WT behaved as a dimer at this concentration (Fig. 2, A and B). At  $6\text{--}12\ \mu\text{M}$ , the mutants eluted in a broader peak of  $\sim 60$  kDa, suggesting an equilibrium between monomer and dimer. By increasing the concentration to  $100\ \mu\text{M}$ , the EFL mutants eluted in a main peak of  $\sim 80$  kDa, matching the values obtained for the WT dimer (12). Using sedimentation velocity analysis,

we estimated that the  $K_d$  for the EFL-2 dimer was  $1.1 \pm 0.4\ \mu\text{M}$ , (Fig. 2C), whereas we had failed to detect the dissociation of the WT dimers under similar conditions (2). These results indicate that the replacement of the flexible loop weakens the dimerization of huDHOase.

We determined the crystal structure of the mutant EFL-2 free of ligands and in complex with DHO or with the inhibitor fluoroorotic acid (FOA). Crystals grown under similar conditions as WT reached  $\sim 0.1$  mm in the maximum dimension and belonged to space group  $\text{C}222_1$  with unit cell dimensions  $a = 82$ ,  $b = 159$ , and  $c = 61\ \text{\AA}$  (Table 1). The crystals diffracted X-rays to resolutions better than  $1.8\ \text{\AA}$  using synchrotron radiation, and the phases were determined by molecular replacement. As reported for the WT (2), the crystals contained one protein subunit/asymmetric unit with a  $V_M$  of  $2.35\ \text{\AA}^3\text{Da}^{-1}$ , and a dimer was formed through a crystallographic 2-fold axis. The electron density is continuous and well-defined for the entire polypeptide chain except for the mutated loop, which can hardly be seen in the structures with DHO or FOA but which clearly adopts an open conformation in the apostructure (Fig. 2, D and E). The rest of the EFL structure is virtually identical to the WT, including the  $\text{Zn}^{2+}$  ions and the bridging water at the

**Table 1**
**Data collection and refinement statistics for apostructures**

Values in parentheses are for the outermost resolution shell. r.m.s., root mean square.

PDB code	Mutants				
	EFL-2	F1563A	F1563T	F1563L	F1563Y
	6HG1	6HFI	6HFE	6HFD	6HFF
<b>Data collection</b>					
Beamline	ID23-1, ESRF	XALOC, ALBA	XALOC, ALBA	XALOC, ALBA	XALOC, ALBA
Wavelength (Å)	1.0	0.9795	0.9795	0.9795	0.9795
Space group	C222 <sub>1</sub>	C222 <sub>1</sub>	C222 <sub>1</sub>	C222 <sub>1</sub>	C222 <sub>1</sub>
Unit cell: <i>a</i> , <i>b</i> , <i>c</i> (Å)	81.1, 160.6, 59.0	81.8, 159.1, 61.3	81.7, 158.7, 61.0	81.6, 158.8, 60.9	81.7, 159.2, 61.1
Resolution (Å)	72.36–2.12 (2.19–2.12)	79.50–1.46 (1.50–1.46)	72.64–1.48 (1.52–1.48)	72.55–1.85 (1.90–1.85)	72.71–1.51 (1.55–1.51)
No. reflections (observed/unique)	144,446/22,259 (13,296/2,197)	449,732/69,387 (31,606/5,050)	436,553/66,300 (32,512/4,859)	221,637/34,137 (16,576/2,507)	411,993/62,751 (30,743/4,608)
Multiplicity	6.5 (6.0)	6.5 (6.3)	6.6 (6.7)	6.5 (6.6)	6.6 (6.7)
<i>R</i> <sub>meas</sub> (%)	8.5 (98.5)	6.2 (71.4)	5.9 (67.7)	8.9 (68.6)	5.5 (68.3)
<i>I</i> / <i>σ</i> <sub>1</sub>	13.3 (2.5)	18.1 (3.1)	17.9 (3.0)	17.8 (3.8)	19.2 (3.7)
Completeness (%)	99.5 (99.2)	99.6 (99.5)	100.0 (99.9)	99.9 (99.9)	100.0 (99.9)
CC <sub>1/2</sub>	99.8 (80.6)	99.9 (90.1)	91.9 (88.5)	99.9 (91.3)	99.9 (91.8)
Wilson B-factor (Å <sup>2</sup> )	41.69	23.3	25.4	31.2	27.6
<b>Refinement</b>					
Resolution (Å)	45.72–2.12	28.25–1.46	30.48–1.48	39.69–1.87	33.34–1.51
No. reflections	22,249	69,425	66,283	33,065	62,741
<i>R</i> -factor/ <i>R</i> <sub>free</sub> (%)	18.03/20.76	12.73/16.38	12.09/15.68	12.15/15.94	12.61/15.11
r.m.s. deviations					
Bond lengths (Å)	0.006	0.009	0.008	0.01	0.011
Bond angles (°)	1.20	1.392	1.327	1.340	1.16
No. atoms (no H)					
Protein + ligand	2,920	2,908	2,905	2,897	2,911
Water	63	391	359	275	308
Ramachandran plot					
Favored (%)	96.45	95.24	96.51	96.53	95.52
Allowed (%)	3.01	4.23	2.95	2.40	3.92
Outliers (%)	0.55	0.53	0.54	1.07	0.56

active site. The DHO and FOA molecules occupy the position described for the WT, although they make an additional interaction with the side chain of Tyr-1558 that adopts a different rotamer (Fig. 2D). Because we could not crystallize the mutant bound to CA-asp, it is unclear whether the *E. coli* flexible loop could reach a closed conformation on the huDHOase active site to favor the reaction (Fig. 2E).

We characterized the activity of mutant EFL-1. As the DHOase reaction is reversible and pH-dependent (2, 22, 23), we thus measured the cyclization of CA-asp to DHO (or forward reaction) at the favored low pH (5.5) and the degradation of DHO (reverse reaction) in alkaline conditions (pH 8). The activity of the mutant is strongly diminished, with turnover rates in the forward ( $k_{\text{cat}}^{\text{CA-asp}} = 1.7 \pm 1.1 \text{ min}^{-1}$ ) and reverse ( $k_{\text{cat}}^{\text{DHO}} = 5.9 \pm 0.9 \text{ min}^{-1}$ ) reactions that are 120- or 50-fold lower, respectively, compared with the WT (Fig. 3, A and B). These results further support the understanding that the flexible loop of huDHOase is key for the reaction and suggest that the *E. coli* flexible loop might not be compatible with the human enzyme.

#### A distinctive phenylalanine in the flexible loop of CAD's DHOase domain is key for catalysis

We then focused on a distinctive feature of the DHOase domain of CAD, the Phe at the tip of the flexible loop. We made three huDHOase mutants substituting Phe-1563 with Thr (mutant F1563T), Leu (F1563L), or Tyr (F1563Y). These variants and the previously reported F1563A mutant were produced as the WT (Fig. S1) and behaved as stable dimers in solution (data not shown).

Mutants F1563A, F1563T, and F1563L show a decreased rate in the forward reaction of 4–8% of the WT, whereas the activity in the reverse reaction is ~1% (Fig. 3, A and B). In turn, mutation F1563Y causes a milder effect, with activities that are 44 and 72% in the forward and reverse reactions, respectively, compared with the WT. The four mutants show a  $K_m^{\text{CA-asp}}$  similar to the WT, and although the low activity did not allow us to measure the  $K_m^{\text{DHO}}$  of mutants F1563A/F1563T/F1563L, the  $K_m^{\text{DHO}}$  of mutant F1563Y was also similar to the WT (Fig. 3, C and D). These results indicate that the reduced catalytic efficiency is not an effect of substrate concentration ( $K_m$ ) but rather a decrease in  $k_{\text{cat}}$  because of the substitution of the conserved Phe residue in the flexible loop.

It is noteworthy that the different Phe-1563 mutations do not affect the forward and reverse reactions equally. As reported for the WT (2), mutant F1563Y is more efficient in catalyzing the forward than the reverse reaction at their optimum pH values, although both rates equilibrate near neutral pH (Fig. 3A). By contrast, mutants F1563A, F1563T, and F1563L show a more detrimental effect in the reverse than in the forward reaction, although as before, the effect on both rates is comparable at pH 7.

#### Structural characterization of huDHOase Phe-1563 mutants

To understand the impact of the mutations on the function of the flexible loop, we determined the structures of the Phe-1563 mutants crystallized in the absence or presence of CA-asp at different pH values. Well-diffracting crystals of the four mutants grew under similar conditions and presented the same space group and unit cell as the WT and EFL-2 mutant (Tables

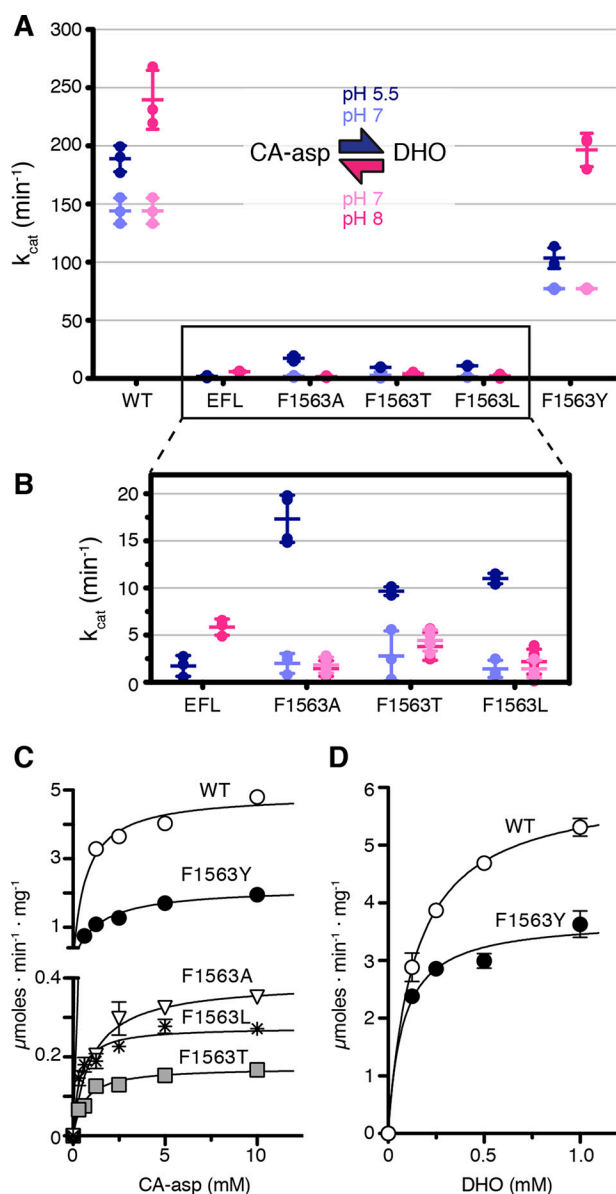


**Figure 3.** A, activities of huDHOase WT and mutants in the forward (blue dots) and reverse (pink dots) reactions measured at pH 5.5 and pH 8, respectively. Activities at pH 7 are overlaid in lighter colors. B, zoom view of less active mutants. C and D, activities at increasing substrate concentrations in the forward (C) and reverse (D) reactions. Data were fitted to a Michaelis-Menten equation. Values are represented as mean  $\pm$  S.D.

1 and 2 and Table S1). The electron density was continuous and well-defined for the entire polypeptide chain (Fig. 4, A–D, and Fig. S3), allowing the building and refinement of the models to correct geometry and reasonable  $R$  and  $R_{free}$  values (Tables 1, 2, and S1).

The overall structures of the mutants are virtually identical to the WT, yielding root-mean-square deviation values of  $<0.11$  Å for the superposition of the complete protein but excluding the flexible loop (Fig. S2). In the apoform, the mutants show the flexible loop in open conformation (Fig. 4, E–H), with the active site filled with solvent and a formate molecule from the crystallization solution that mimics the interactions of the  $\alpha$ -COOH group of CA-asp or DHO with the side chains of residues Asn-1505, Arg-1475, and His-1690 (Fig. S3) (2).

The structures of mutants F1563A, F1563T, and F1563L co-crystallized with CA-asp at different pH values (6.5, 7.0, and 7.5) (Tables 2 and S1) show a molecule of DHO bound in the active site with full occupancy and, accordingly, present the flexible loop in the open conformation (Fig. 4, A–C and E–G). The flexible loop is not involved in lattice contacts, and thus we excluded the probability that the loop-out conformation could be favored by crystal packing. In contrast, the structure of mutant F1563Y co-crystallized with CA-asp (at pH 6.5, 7.0, or 7.5) exhibits a molecule of this ligand within the active site (Fig. 4, D and H), with the flexible loop in the closed conformation and the side chain of Thr-1562 interacting with the  $\beta$ -COOH group of CA-asp (Fig. 5A). The mutated Tyr occupies virtually the same position as Phe-1563 in the WT and makes a H-bond through the carbonyl oxygen with the side chain of Asn-1505 and van der Waals contacts with the  $\alpha$ -COOH group of CA-asp and with residues His-1690, Arg-1475, Pro-1701, and Pro-1702 (Fig. 5, A and C). As observed in the WT, the aromatic ring of the mutated Tyr falls on top of the side chain of His-1690 and favors cation– $\pi$  interactions with the side chains of residues Arg-1475 and Arg-1507. In addition, the phenolic oxygen of Tyr allows two extra H-bonds with the side chain of Arg-1507 and with an ordered water molecule.

However, the position of the mutated Tyr is different from the position of Phe-1563 in the WT apostructures (Fig. 5, B and D). In the open conformation, the side chain of Phe-1563 is in close proximity to the  $\beta 2$ – $\alpha 2$  loop, making a planar stacking interaction with the side chain of Arg-1507 (Fig. 5D). In this position, the phenolic oxygen of the mutated Tyr would clash with the carbonyl oxygen atom of Asn-1505, and thus the side chain is oriented in an opposite direction (Fig. 5B). This readjustment of the flexible loop correlates with a partial disorder in the side chain of Tyr-1558 that adopts two alternate conformations, one as in the WT and the other pointing toward the substrate, as seen in the EFL-2 mutant (Figs. 2E and 5B).

The structural comparison between the mutants and the WT did not reveal any other significant differences in the orientation of the substrates, the position of the catalytic residues, or the coordination of the  $Zn^{2+}$  ions at the active site. Thus, we concluded that the nature of the residue occupying the position of Phe-1563 affects the conformation of the flexible loop and is responsible for the differences in activity and for the exclusive binding of CA-asp or DHO to the active site of the protein in the crystal.

### Simulation of the loop fluctuation by molecular dynamics

We further interrogated the role of Phe-1563 by comparing the movements of the loop in the WT and F1563A mutant using molecular dynamics (MD). The simulations started with both proteins having DHO in the active site and the flexible loop in open conformation. Interestingly, the loop in the WT was able to sample closed conformations. Contrary, the mutated loop did not reach conformations compatible with the closed state, remaining highly flexible and quite far from the active site. The analysis of the distances between the loop and the DHO quantitatively shows such differences between the two protein conformational behaviors (Fig. 6A). In the WT, the mode of the distribution (*i.e.* the most probable value) of the distance

**Table 2**
**Data collection and refinement statistics for structures with CA-asp/DHO at pH 7.0**

Values in parentheses are for the outermost resolution shell. r.m.s., root mean square.

PDB code	Mutants				
	EFL-2	F1563A	F1563T	F1563L	F1563Y
	6HG3	6HFH	6HFP	6HFL	6HFR
<b>Data collection</b>					
Beamline	ID23-1, ESRF	PETRA III--DESY	PETRA III--DESY	PETRA III--DESY	PETRA III--DESY
Wavelength (Å)	1.0	1.0	1.0	1.0	1.0
Space group	C222 <sub>1</sub>	C222 <sub>1</sub>	C222 <sub>1</sub>	C222 <sub>1</sub>	C222 <sub>1</sub>
Unit cell: <i>a</i> , <i>b</i> , <i>c</i> (Å)	81.9, 159.5, 61.9	82.0, 159.1, 61.6	82.1, 159.0, 61.2	82.0, 158.8, 61.2	81.9, 159.1, 61.0
Resolution (Å)	48.88–1.97 (2.04–1.97)	36.45–1.45 (1.50–1.45)	46.89–1.20 (1.24–1.20)	40.97–1.35 (1.40–1.35)	46.75–1.30 (1.35–1.30)
No. reflections (observed/unique)	188,663/28,867 (19,918/2,883)	468,465/71,360 (40,311/6,886)	800,184/124,981 (75,046/12,167)	564,836/87,621 (53,868/8,637)	641,051/97,702 (56,548/9,576)
Multiplicity	6.5 (6.9)	6.6 (5.9)	6.4 (6.2)	6.4 (6.2)	6.6 (5.9)
<i>R</i> <sub>meas</sub> (%)	6.2 (45.6)	7.3 (75.8)	4.6 (67.0)	4.6 (68.5)	4.4 (62.2)
<i>I</i> / <i>σ</i> <sub><i>I</i></sub>	19.4 (3.7)	16.9 (2.4)	21.6 (2.6)	22.3 (2.4)	21.9 (2.6)
Completeness (%)	98.3 (99.6)	99.4 (97.0)	99.6 (97.8)	99.8 (99.5)	99.7 (99.2)
CC <sub>1/2</sub>	99.9 (92.5)	99.9 (82.7)	99.9 (87.0)	1.0 (81.9)	99.9 (89.4)
Wilson B-factor (Å <sup>2</sup> )	30.50	14.0	13.2	15.4	15.9
<b>Refinement</b>					
Resolution (Å)	48.88–1.97	36.45–1.45	46.89–1.20	40.97–1.35	46.75–1.30
No. reflections	28,661	71,346	124,950	87,611	97,685
<i>R</i> -factor/ <i>R</i> <sub>free</sub> (%)	16.12/17.79	11.81/14.26	12.20/13.69	11.85/13.63	12.64/14.40
r.m.s. deviations					
Bond lengths (Å)	0.007	0.008	0.011	0.011	0.01
Bond angles (°)	1.32	1.00	1.190	1.120	1.09
No. atoms (no H)					
Protein + ligand	2,842	2,911	2,941	2,901	2,940
Water	293	429	513	422	364
Ramachandran plot					
Favored (%)	96.61	95.53	96.08	95.80	95.80
Allowed (%)	3.11	3.91	3.36	3.64	3.64
Outliers (%)	0.28	0.56	0.56	0.56	0.56

between the Cα of residue 1563 and DHO is ~5 Å, corresponding to the closed or nearly closed state, and presents a second minor peak at 10 Å that corresponds to the open conformation. In turn, mutant F1563A shows a distribution centered at 10 Å, indicating that during the simulation, the mutated loop did not reach the closed state. The analysis of the fluctuations shows a different behavior for the dynamics of the loop, with the fluctuations being more pronounced in the mutated system (Fig. 6B). This is explained by the WT loop, which, early in the simulation, becomes stabilized in a closed state, thus reducing its fluctuations.

## Discussion

### Unique features in the flexible loop of CAD's DHOase domain

Despite evolutionary divergence, the structure of huDHOase revealed a striking similarity to the active site of ecDHOase (2). Not only do the catalytic elements occupy virtually identical positions in both enzymes, but also no significant changes were observed whether the active sites were free or bound to the substrates or to specific inhibitors. This preservation and rigidity of the active site is only broken by the flexible loop and its lid movement, which appears tightly coupled to the catalytic state of the enzyme (Fig. 1, D and E) (2, 17). The flexible loop in the DHOase domain of CAD shares only one Thr with the equivalent loop of *E. coli* and other bacterial type II DHOases (human Thr-1562 and *E. coli* Thr-109) (Fig. 1C). Nevertheless, upon CA-asp binding and lid closure, the invariant Thr takes the same position and interacts in the same manner with the substrate both in the human and *E. coli* proteins (2, 16). Considering the similar arrangement of the catalytic elements, we found

it intriguing that the activity of huDHOase is ~50-fold lower than the *E. coli* enzyme (2, 16). This difference could be because of small unnoticed movements (<1 Å) in the active site elements that affect catalysis (24) but also because of different interactions of the flexible loop with the substrate and the dynamics of the flexible loop itself.

In ecDHOase, a Thr (Thr-110) occupying the tip of the flexible loop makes an extra H-bond with CA-asp, whereas in CAD, the Phe at this position (Phe-1563) cannot make a similar interaction with the substrate (Fig. 1, C–E). Interestingly, the damaging effect of mutation T110A makes the activity of ecDHOase more similar to that of the human enzyme (16). To test whether an additional H-bond with CA-asp would increase the activity of huDHOase, we replaced the flexible loop of huDHOase with the equivalent sequence in the *E. coli* enzyme. However, rather than enhancing the reaction, the EFL chimera was inactive (Fig. 3, A and B). This bold mutation also destabilized the formation of the dimers (Fig. 2, A–C), indicating that the contribution of the residues at the hinge of the flexible loop (Leu-1559, Asn-1560, and Asp-1569) to the intersubunit contacts might be more relevant than initially thought (2) (Fig. 1C).

This result also stresses an interesting difference with ecDHOase. In the bacterial enzyme, dimerization occurs by interactions of the loops adjoining the flexible loop above the β-barrel rather than by lateral contacts as in huDHOase (2, 14, 17) (Fig. S4). Moreover, ecDHOase shows a strong cooperativity between the two active sites (17), consistent with an asymmetry in the crystal structures, with one subunit having CA-asp bound at the active site and the other DHO (14, 17). Indeed, it

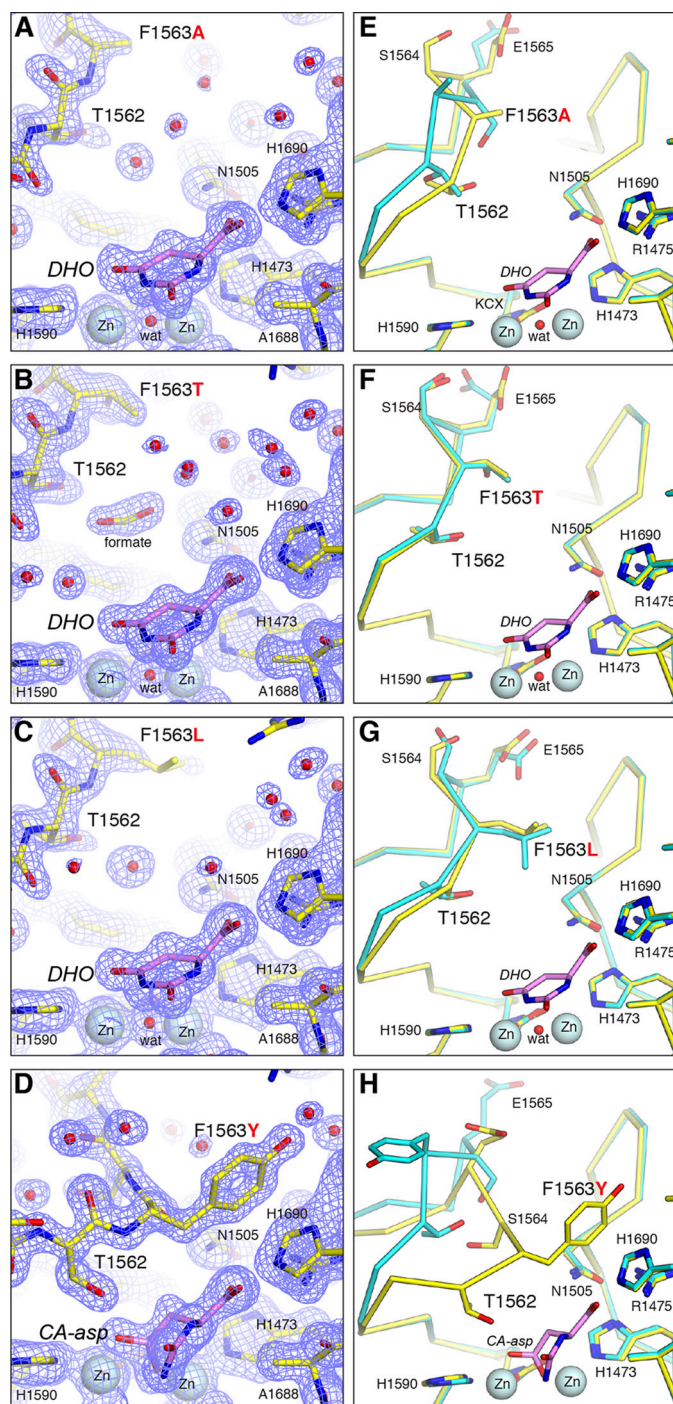


**Figure 4.** A–D, active sites in the crystal structures of mutants F1563A (A), F1563T (B), F1563L (C), and F1563Y (D) with  $2F_{\text{obs}} - F_{\text{calc}}$  electron density map. A molecule of DHO (A–C) or CA-asp (D) is shown with carbon atoms in magenta. Water molecules and  $\text{Zn}^{2+}$  ions are represented as red and light cyan spheres, respectively. E–H, views of the active site with superposition of the apo (cyan) and ligand-bound (yellow) structures.

has been proposed that the binding of CA-asp or DHO and the accompanying movement of the flexible loop could correlate with changes in the dimerization interface of ecDHOase, allowing the communication between subunits (17). One the contrary, in huDHOase we did not detect cooperativity, and the binding of CA-asp or DHO to one subunit does not appear to condition the active site content in the other subunit (2). Per-

haps the two additional residues in the ecDHOase flexible loop and the larger amplitude of its movement compared with huDHOase (Fig. 1, D and E) could be required for interaction with the dimerization elements.

Swapping the entire flexible loop must distort the dimerization interface of huDHOase, which could explain at least part of the detrimental effect on the activity. Indeed, monomeric huDHOase mutants are reported to be 2-fold less active than the WT (2). However, the negligible activity of the protein chimera likely responds to a lack of complementarity between the *E. coli* loop and the huDHOase active site. Although, we initially thought that perhaps a shorter or longer *E. coli* sequence would allow the closure and precise positioning of the loop for catalysis, the following experiment proved that this might not be the case. We demonstrated that the single substitution of Phe-1563 with the Thr present in *E. coli* and all bacterial type II DHOases was sufficient to damage huDHOase activity (Fig. 3, A and B). This result suggests that the importance of the residue at the tip of the flexible loop goes beyond its ability to form a H-bond with the substrate. Indeed, it is reported that in ecDHOase, substitution of Thr-110 with Val only decreases the activity to 80%, whereas substitution with Ser, which retains the H-bond with CA-asp, has a more damaging effect, decreasing the activity to 33% (16). Overall, these data support the view that there must exist a complementarity between the residue at the tip of the flexible loop and other active site elements. In fact, we proved that Phe-1563 can be replaced by a Tyr with only mild effects on the activity of huDHOase (Fig. 3) but not by a Leu, indicating that the aromatic ring at the side chain, and not only its hydrophobic character, is important for the correct functioning of the loop. This result brings attention to the relevance of the cation- $\pi$  interactions among Phe-1563 and Arg-1475 and Arg-1507 for the stabilization of the loop in the closed conformation and to the planar stacking interaction of Phe-1563 with Arg-1507 in the open state (Fig. 5), both of which went unnoticed in previous structural work (2). Altogether, our results confirm the key participation of the flexible loop in the activity of CAD's DHOase domain, proving that despite sharing a conserved catalytic role, the flexible loop stands as the most dissimilar active site element, being characteristic of and likely irreplaceable for each DHOase group.

#### Phe-1563 is a secure grip that stabilizes the closure of the flexible loop

Given the reversibility of the DHOase reaction, we expected that, similar to what occurred with the WT, the crystal structures of the Phe-1563 mutants would present an average electron density in the active site corresponding to a mixture of CA-asp and DHO and to the flexible loop in the two alternate conformations (2). Thus, we found it surprising that the structures of mutants F1563A/F1563T/F1563L had the loop open and DHO bound with full occupancy in the active site, whereas mutant F1563Y crystallized exclusively with the loop closed and with CA-asp (Fig. 4, A–D). These structures strongly suggest that the interactions of Phe-1563 are key for the conformational equilibrium between the two catalytic states of the protein. The MD data support this hypothesis, showing that without the Phe, the flexible loop is not stabilized over the substrate and remains in an open conformation during the simu-

## A catalytic flexible loop in the DHOase domain of human CAD

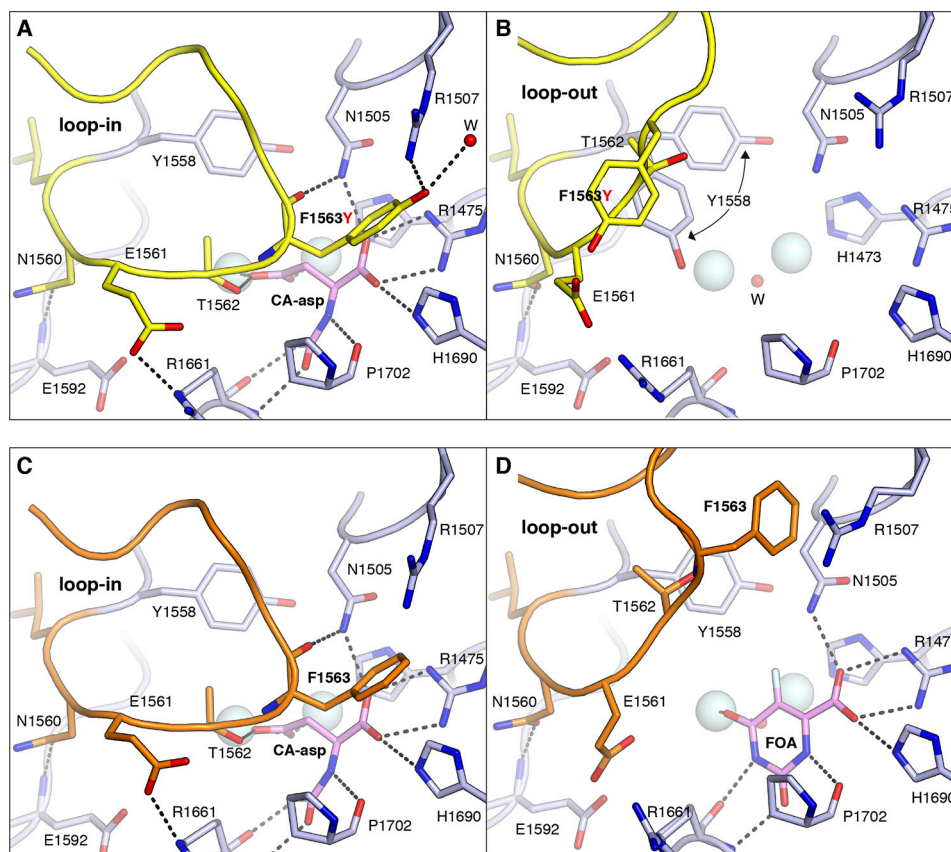


**Figure 5.** A and B, cartoon representation of the active site of huDHOase F1563Y bound to CA-aspartate (A) or in apoform (B). The flexible loop is colored with C atoms in yellow. Other residues in the active site are colored with C atoms in light blue. CA-aspartate is colored with C atoms in pink. C and D, WT structures bound to CA-aspartate (C) or FOA (D) with the flexible loop shown in orange.

lation (Fig. 6A). Our data further prove that the lack of closure is not an impediment to proper binding of DHO, as shown by the nearly identical position occupied by this substrate in the structures of the F1563A/F1563T/F1563L mutants (Fig. 4, A–C). This would explain that, despite low activity, the DHO produced during the crystallization binds preferentially to the open active site of the F1563A/F1563T/F1563L mutants. On the other hand, because Tyr mimics the hydrophobic and cation– $\pi$  interactions of Phe-1563 (Fig. 5), we postulate that mutant F1563Y must tend to reach the closed state in a manner similar to the WT (Fig. 6) and that the additional interactions of the phenolic oxygen may increase the stability of the loop-in conformation, favoring the notion that the crystals show this active site arrangement exclusively (Figs. 4D and 5A). Because no other differences were observed between the structures of the mutants free or bound to the substrate and the WT protein, we concluded that the lack of closure (mutants F1563A/F1563T/F1563L) or the additional stabilization in the closed state (mutant F1563Y) hamper the dynamic fluctuations of the flexible loop-in and -out of the active site, causing the diminished activity of the mutants.

The observation that the WT and mutant F1563Y show a faster rate in the reverse than in the forward reaction (measured at their respective optimum pH), whereas mutations F1563A/F1563T/F1563L show an opposite trend (Fig. 3, A and B), leads to a further question as to how the grip of the Phe aids during catalysis. According to the proposed catalytic mechanism (14,

16–18), the biosynthesis of DHO starts by the removal of the water molecule bridging the two  $\text{Zn}^{2+}$  ions to allow binding of CA-aspartate, which induces the closure of the flexible loop. Based on the present data, we propose that the interaction between the side chain of Thr-1562 and the  $\beta$ -COOH of CA-aspartate is not sufficient to stabilize the loop-in conformation and that the anchoring of Phe-1563 is mandatory to confine the substrate at the active site to enhance the nucleophilic attack of the nitrogen atom to the  $\beta$ -COOH group and to stabilize the transition state of the reaction (Fig. 1B). Then, upon cyclization, the  $\beta$ -COOH group is converted to a carbonyl group and to a hydroxide ion that remains bound to the  $\text{Zn}^{2+}$  ions (Fig. 1B), whereas the DHO moves away from the metals, causing a steric pressure on residue Thr-1562 and “pushing” the flexible loop to the open conformation to allow product release and the beginning of a new reaction cycle (17, 18). Thus, our findings suggest that mutations affecting the closure of the flexible loop can be detrimental either because they impair the interactions and decrease the frequency with which the loop reaches the stable closed conformation (EFL and F1563A/F1563T/F1563L mutants) or because they provide a stronger grip that counteracts the pushing of the DHO and hinders the opening and release of the product (F1563Y).

In the reverse reaction, the degradation of DHO involves the deprotonation of the water molecule bridging the metal ions and further nucleophilic attack on the DHO ring (Fig. 1B), which follows the same mechanistic steps as before but in

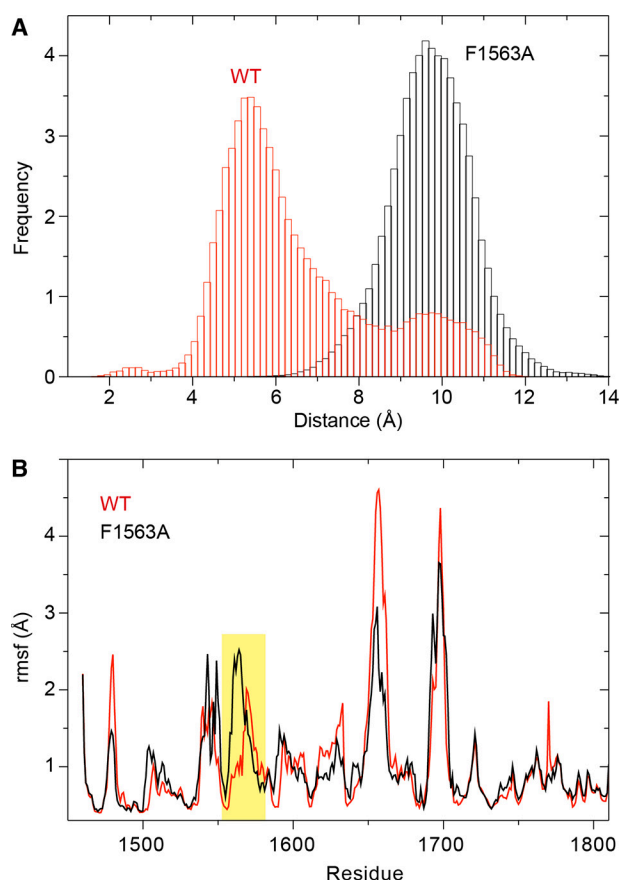


**Figure 6.** A, distributions of distances between the C $\alpha$  of residue 1563 and DHO for the WT (red lines) and F1563A mutant (black lines) as obtained by the corresponding MD simulations. B, RMSF for WT (red lines) and F1563A mutant (black lines) as obtained by the corresponding MD simulations. The area highlighted in yellow corresponds to the region of the flexible loop.

the opposite order. As seen in the structures of the F1563A/F1563T/F1563L and EFL mutants, DHO enters into the active site and does not require the interaction with the flexible loop for correct binding. Then, the loop must close over the active site, as observed in the MD simulations of the WT, and “push” the DHO ring into close proximity to the bridging water to favor the nucleophilic attack. In this case, there is no interaction between Thr-1562 and the missing  $\beta$ -COOH group of DHO; thus, Phe-1563 must play a key role in promoting the closure of the loop and in introducing steric strain between the DHO and the attacking water. The negligible rate of the F1563A/F1563T/F1563L mutants in the reverse reaction likely reflects the failure of the flexible loop to compress the substrates and highlights the prominent role of Phe-1563 in configuring the active site of CAD’s DHOase domain and in promoting catalysis.

This study highlights an important difference between human and bacterial DHOases. It also lends further insight for the future development of inhibitory compounds that, mimicking the effect of the mutations reported here, could block the closure or opening of the flexible loop.

## Experimental procedures

### Site-directed mutagenesis

Mutagenesis was carried out by primer extension, incorporating mutagenic primers in independently nested PCRs before

combining them in the final product in a second round of PCR using specific flanking primers (25). The primer sequences are detailed in Table S2. The cDNA of human CAD (UniProt P27708) purchased from Open Biosystems (clone ID 5551082) was used as the template for the mutagenesis. Gene amplification was carried out with Phusion High-Fidelity DNA polymerase (New England Biolabs). The amplified mutated genes were inserted into the pOPIN-M expression vector (Oxford Protein Production Facility) using In-Fusion technology (Clontech). This vector tags the N terminus of the protein with a His<sub>6</sub>-tagged maltose-binding protein (His<sub>6</sub>-MBP) followed by a specific cleavage site for protease PreScission. The resulting plasmids with the desired gene mutations were verified by sequencing. Mutant EFL-1 was generated by four successive rounds of mutagenesis using the pairs of primers listed in Table S2. Mutant EFL-2 was generated from the EFL-1 reverting the mutation L1559P back to Leu.

### Protein production

Mutated forms of huDHOase were expressed and purified as reported previously (2, 12). The proteins were produced in HEK293S-GnTI cells adapted to suspension culture in Free-Style medium (Invitrogen) with 1% fetal bovine serum and grown in an orbital stirrer at 135 rpm under standard humidified conditions (26). The cultures (1.5 million cells/ml) were transfected with the pOPIN-M vectors carrying the mutated huDHOase genes in a 1:3 ratio mixture of DNA (1 mg/ml) and polyethylenimine (25 kDa branched, Sigma). Prior to the transfection, DNA and polyethylenimine were diluted to 20 and 60 mg/ml, respectively, in UltraDOMA medium (Lonza) and incubated separately for 5 min at room temperature. Then, the solutions were mixed and incubated for 10 min before adding the mixture to the cells, which were harvested after 2–3 days and stored at  $-80^{\circ}\text{C}$ . For purification, the cells were thawed and resuspended in buffer A (20 mM Tris-HCl, pH 8, 0.5 M NaCl, 10 mM imidazole, 5% glycerol, and 2 mM  $\beta$ -mercaptoethanol) with 2 mM phenylmethanesulfonyl fluoride and disrupted in a Dounce homogenizer followed by brief sonication. The clarified lysate was applied onto a 5-ml Ni<sup>2+</sup>-loaded HisTrap FF chelating column (GE Healthcare). Following extensive washing with buffer A containing 25 mM imidazole, the protein was eluted with buffer A supplemented with 250 mM imidazole. Excess imidazole was removed by overnight dialysis against the same solution containing 30 mM imidazole with the inclusion of GST-tagged PreScission protease (1/20th of the protein weight) within the dialysis bag to cleave off the His<sub>6</sub>-MBP tag. Then, the sample was reloaded onto a HisTrap column connected to a 5-ml GSTrap FF column (GE Healthcare) to retain the non-cleaved protein, the His<sub>6</sub>-MBP tag, and the GST-tagged protease. The untagged huDHOase found in the columns flow-through was concentrated to 3 mg ml<sup>-1</sup> using an Amicon Ultra system with a 10-kDa cutoff membrane and further purified by SEC on a Superdex 200 10/300 column (GE Healthcare) equilibrated with GF buffer (20 mM Tris, pH 8, 0.15 M NaCl, 20  $\mu\text{M}$  ZnSO<sub>4</sub>, and 0.2 mM TCEP). For the EFL mutants, the NaCl concentration in the GF buffer was increased to 0.25 M. The mutated proteins eluted as single peaks that were pooled and concentrated as described above to 3 mg ml<sup>-1</sup> and used directly

## A catalytic flexible loop in the DHOase domain of human CAD

for crystallization studies. The excess protein was supplemented with 20% glycerol, flash-frozen in liquid nitrogen prior to SEC, and stored at 193 K for several weeks. Freezing did not have a noticeable effect either on the crystallization or on the specific activity. All purification steps were carried out at 277 K. Protein concentration was determined from the absorbance at 280 nm using a theoretical extinction coefficient of  $38,960 \text{ M}^{-1} \text{ cm}^{-1}$ .

### Crystallization, data collection, and structure determination

Crystals of the EFL and Phe-1563 mutants, alone or in the presence of 4 mM DHO, CA-asp, or FOA, were obtained as reported previously for the WT (2, 12). Optimal crystallization conditions were similar for all the mutants and consisted of 2–3 mg ml<sup>-1</sup> protein in GF buffer with 2.5–3 M sodium formate and 0.1 M HEPES, pH 6.5–7.5, as the mother liquor. Prior to flash-freezing, the crystals were transferred to cryoprotectant solutions containing increasing amounts of glycerol, up to a final concentration of 15%, and 20  $\mu\text{M}$  ZnSO<sub>4</sub>. For the crystals grown in the presence of ligands, the compound was also added to the cryoprotectant solutions at a final concentration of 4 mM. X-ray diffraction datasets were collected at PETRA-III (DESY, Hamburg, Germany), XALOC (ALBA Synchrotron, Barcelona, Spain), or ID23-1 (ESRF, Grenoble, France) using Pilatus 6M detectors. Data processing and scaling were performed with XDS (27) and autoPROC (28). Crystallographic phases were obtained by molecular replacement using PHASER (29) and the structure of huDHOase WT (PDB entries 4C6C (apo) and 4C6I (DHO-bound)) as the search models. The models were constructed by iterative cycles of model building in COOT (30) and refinement in PHENIX (31) or Refmac5 in CCP4 (32, 33).

### Enzymatic assays

DHOase activity was assayed spectrophotometrically following the production or degradation of DHO by absorbance at 230 nm as detailed elsewhere (2). Reactions were carried out at 25 °C in a final volume of 100  $\mu\text{l}$  containing 50 mM sodium phosphate (at pH 5.5, 7, or 8), 150 mM NaCl, 20  $\mu\text{M}$  ZnSO<sub>4</sub>, 0.1 mg/ml BSA, and 0.5 mM DHO or 5 mM CA-asp. Protein concentrations were 0.25  $\mu\text{M}$  for the WT and 2.5–3  $\mu\text{M}$  for the mutants. Kinetic data analysis was performed with GraphPad Prism.

### SEC-MALS

400  $\mu\text{l}$  of purified protein at different concentrations (WT: 1.2  $\mu\text{M}$ ; EFL-1: 120, 12, and 1.2  $\mu\text{M}$ ; EFL-2: 93, 6, and 1.2  $\mu\text{M}$ ) was fractionated on a Superdex 200 10/300 column equilibrated in GF buffer using an AKTA purifier (GE-Healthcare). The eluted samples were characterized by in-line measurement of the refractive index and multi-angle light scattering using Optilab T-rEX and DAWN 8+ instruments, respectively (Wyatt Technology). Data were analyzed with ASTRA 6 software (34) and plotted with GraphPad.

### Analytical centrifugation

Sedimentation velocity studies were performed using a Beckman XL-I centrifuge, an An-50 Ti rotor, and a 12-m double-sector centerpiece. The absorbance at 230 nm was measured to

follow the distribution of the sedimenting molecules at 42,000 rpm and 293 K. Sedimentation coefficient distributions were calculated using SEDFIT 15.01b (35). Purified EFL-2 mutant samples were in GF buffer at concentrations of 14, 9.3, 4.6, 2.3, 1.2, and 0.6  $\mu\text{M}$ .

### Molecular dynamics

MD simulations of the WT and F1563A proteins were performed using the corresponding X-ray structures as starting models. The simulations started with both proteins having DHO in the active site and the flexible loop in open conformation. MD simulations in the NVT ensemble (constant number (N), volume (V) and temperature (T)) (constant temperature and volume), with fixed bond lengths and a time step of 2 fs for numerical integration, were performed with the GROMACS software package (36). The GROMOS force field (37) has been used for the proteins, whereas the DHO molecule has been modeled by means of the ATB server (38). Water was modeled by the simple point charge (SPC) model. A nonbond pair list cutoff of 9.0 Å was used, and the pair list was updated every four time steps. The long-range electrostatic interactions were treated with the particle mesh Ewald method (39). The v-rescale temperature coupling (40) was used to keep the temperature constant at 300 K. The proteins were solvated with water and placed in a periodic truncated octahedron large enough to contain the proteins and  $\sim 1.0$  nm of solvent on all sides. Counterions were added by replacing a corresponding number of water molecules to achieve a neutral condition. The side chains were protonated so as to reproduce a pH of  $\sim 7$ .

**Author contributions**—F. d. C.-O., A. G.-G., M. D., and S. R.-M. formal analysis; F. d. C.-O., A. G.-G., M. R.-L., M. D., and S. R.-M. investigation; F. d. C.-O., A. G.-G., M. R.-L., M. D., and S. R.-M. writing-review and editing; M. D. and S. R.-M. conceptualization; S. R.-M. supervision; S. R.-M. funding acquisition; S. R.-M. writing-original draft.

**Acknowledgments**—X-ray diffraction experiments were performed at XALOC beamline at the ALBA Synchrotron with the collaboration of the ALBA staff and CALIPSOplus (Grant 730872) funding, at PETRA III beamline at DESY with the assistance of Michele Cianci and Sarah Marshall, or at beamline ID23-1 at the ESRF as part of the Block Allocation Group (BAG) Proposal MX1842. SEC-MALS analyses were performed at the Spanish National Cancer Research Centre (CNIO) with the support of Drs. Ramón Campos-Olivas and Clara M. Santiveri. Institutional grants from the Fundación Ramón Areces and Banco de Santander to the CBMSO are also acknowledged.

### References

1. Jones, M. E. (1980) Pyrimidine nucleotide biosynthesis in animals: genes, enzymes, and regulation of UMP biosynthesis. *Annu. Rev. Biochem.* **49**, 253–279 [CrossRef Medline](#)
2. Grande-García, A., Lallous, N., Diaz-Tejada, C., and Ramón-Maiques, S. (2014) Structure, functional characterization, and evolution of the dihydroorotase domain of human CAD. *Structure* **22**, 185–198 [CrossRef Medline](#)
3. Fields, C., Brichta, D., Shepherdson, M., Farinha, M., and O'Donovan, G. (1999) Phylogenetic analysis and classification of dihydroorotases: A complex history for a complex enzyme. *Paths to Pyrimidines* **7**, 49–63
4. Brooke, J., Szabados, E., Lyons, S. D., Goodridge, R. J., Harsanyi, M. C., Poiner, A., and Christopherson, R. I. (1990) Cytotoxic effects of dihydro-

- orotase inhibitors upon human CCRF-CEM leukemia. *Cancer Res.* **50**, 7793–7798 [Medline](#)
5. Cassera, M. B., Zhang, Y., Hazleton, K. Z., and Schramm, V. L. (2011) Purine and pyrimidine pathways as targets in *Plasmodium falciparum*. *Curr. Top. Med. Chem.* **11**, 2103–2115 [CrossRef Medline](#)
6. Christopherson, R. I., Lyons, S. D., and Wilson, P. K. (2002) Inhibitors of *de novo* nucleotide biosynthesis as drugs. *Acc. Chem. Res.* **35**, 961–971 [CrossRef Medline](#)
7. Li, Y., and Raushel, F. M. (2005) Inhibitors designed for the active site of dihydroorotase. *Bioorg. Chem.* **33**, 470–483 [CrossRef Medline](#)
8. Schroeder, P. E., Patel, D., and Hasinoff, B. B. (2008) The dihydroorotase inhibitor 5-aminoorotic acid inhibits the metabolism in the rat of the cardioprotective drug dextrazoxane and its one-ring open metabolites. *Drug Metab. Dispos.* **36**, 1780–1785 [CrossRef Medline](#)
9. Coleman, P. F., Suttle, D. P., and Stark, G. R. (1977) Purification from hamster cells of the multifunctional protein that initiates *de novo* synthesis of pyrimidine nucleotides. *J. Biol. Chem.* **252**, 6379–6385 [Medline](#)
10. Lee, L., Kelly, R. E., Pastra-Landis, S. C., and Evans, D. R. (1985) Oligomeric structure of the multifunctional protein CAD that initiates pyrimidine biosynthesis in mammalian cells. *Proc. Natl. Acad. Sci. U.S.A.* **82**, 6802–6806 [CrossRef Medline](#)
11. Evans, D. R., and Guy, H. I. (2004) Mammalian pyrimidine biosynthesis: fresh insights into an ancient pathway. *J. Biol. Chem.* **279**, 33035–33038 [CrossRef Medline](#)
12. Lallous, N., Grande-Garcia, A., Molina, R., and Ramon-Maiques, S. (2012) Expression, purification, crystallization and preliminary X-ray diffraction analysis of the dihydroorotase domain of human CAD. *Acta Crystallogr. Sect. F Struct. Biol. Cryst. Commun.* **68**, 1341–1345 [CrossRef Medline](#)
13. Seibert, C. M., and Raushel, F. M. (2005) Structural and catalytic diversity within the amidohydrolase superfamily. *Biochemistry* **44**, 6383–6391 [CrossRef Medline](#)
14. Thoden, J. B., Phillips, G. N., Jr, Neal, T. M., Raushel, F. M., and Holden, H. M. (2001) Molecular structure of dihydroorotase: A paradigm for catalysis through the use of a binuclear metal center. *Biochemistry* **40**, 6989–6997 [CrossRef Medline](#)
15. Ruiz-Ramos, A., Grande-García, A., and Ramón-Maiques, S. (2015) Dihydroorotase domain of human CAD. In *Encyclopedia of Inorganic and Bioinorganic Chemistry*, (Scott, R. A., ed), John Wiley & Sons, Hoboken, NJ 10.1002/9781119951438.eibc2321 [CrossRef](#)
16. Lee, M., Maher, M. J., Christopherson, R. I., and Guss, J. M. (2007) Kinetic and structural analysis of mutant *Escherichia coli* dihydroorotases: A flexible loop stabilizes the transition state. *Biochemistry* **46**, 10538–10550 [CrossRef Medline](#)
17. Lee, M., Chan, C. W., Mitchell Guss, J., Christopherson, R. I., and Maher, M. J. (2005) Dihydroorotase from *Escherichia coli*: Loop movement and cooperativity between subunits. *J. Mol. Biol.* **348**, 523–533 [CrossRef Medline](#)
18. Lee, M., Chan, C. W., Graham, S. C., Christopherson, R. I., Guss, J. M., and Maher, M. J. (2007) Structures of ligand-free and inhibitor complexes of dihydroorotase from *Escherichia coli*: Implications for loop movement in inhibitor design. *J. Mol. Biol.* **370**, 812–825 [CrossRef Medline](#)
19. Rice, A. J., Lei, H., Santarsiero, B. D., Lee, H., and Johnson, M. E. (2016) Ca-asp bound X-ray structure and inhibition of *Bacillus anthracis* dihydroorotase (DHOase). *Bioorg. Med. Chem.* **24**, 4536–4543 [CrossRef Medline](#)
20. Zhang, P., Martin, P. D., Purcarea, C., Vaishnav, A., Brunzelle, J. S., Fernando, R., Guy-Evans, H. I., Evans, D. R., and Edwards, B. F. (2009) Dihydroorotase from the hyperthermophile *Aquifex aeolicus* is activated by stoichiometric association with aspartate transcarbamoylase and forms a one-pot reactor for pyrimidine biosynthesis. *Biochemistry* **48**, 766–778 [CrossRef Medline](#)
21. Evans, H. G., Fernando, R., Vaishnav, A., Kotichukkala, M., Heyl, D., Hachem, F., Brunzelle, J. S., Edwards, B. F., and Evans, D. R. (2014) Intersubunit communication in the dihydroorotase-aspartate transcarbamoylase complex of *Aquifex aeolicus*. *Protein Sci.* **23**, 100–109 [CrossRef Medline](#)
22. Christopherson, R. I., and Jones, M. E. (1979) Interconversion of carbamyl-L-aspartate and L-dihydroorotate by dihydroorotase from mouse Ehrlich ascites carcinoma. *J. Biol. Chem.* **254**, 12506–12512 [Medline](#)
23. Porter, T. N., Li, Y., and Raushel, F. M. (2004) Mechanism of the dihydroorotase reaction. *Biochemistry* **43**, 16285–16292 [CrossRef Medline](#)
24. Koshland, D. E., Jr. (1998) Conformational changes: How small is big enough? *Nat. Med.* **4**, 1112–1114 [CrossRef Medline](#)
25. Ho, S. N., Hunt, H. D., Horton, R. M., Pullen, J. K., and Pease, L. R. (1989) Site-directed mutagenesis by overlap extension using the polymerase chain reaction. *Gene* **77**, 51–59 [CrossRef Medline](#)
26. Aricescu, A. R., Lu, W., and Jones, E. Y. (2006) A time- and cost-efficient system for high-level protein production in mammalian cells. *Acta Crystallogr. D Biol. Crystallogr.* **62**, 1243–1250 [CrossRef Medline](#)
27. Kabsch, W. (2010) XDS. *Acta Crystallogr. D Biol. Crystallogr.* **66**, 125–132 [CrossRef Medline](#)
28. Vonrhein, C., Flensburg, C., Keller, P., Sharff, A., Smart, O., Paciorek, W., Womack, T., and Bricogne, G. (2011) Data processing and analysis with the autoPROC toolbox. *Acta Crystallogr. D Biol. Crystallogr.* **67**, 293–302 [CrossRef Medline](#)
29. McCoy, A. J., Grosse-Kunstleve, R. W., Adams, P. D., Winn, M. D., Storoni, L. C., and Read, R. J. (2007) Phaser crystallographic software. *J. Appl. Crystallogr.* **40**, 658–674 [CrossRef Medline](#)
30. Emsley, P., Lohkamp, B., Scott, W. G., and Cowtan, K. (2010) Features and development of Coot. *Acta Crystallogr. D Biol. Crystallogr.* **66**, 486–501 [CrossRef Medline](#)
31. Adams, P. D., Afonine, P. V., Bunkóczi, G., Chen, V. B., Davis, I. W., Echols, N., Headd, J. J., Hung, L. W., Kapral, G. J., and Grosse-Kunstleve, R. W. (2010) PHENIX: A comprehensive Python-based system for macromolecular structure solution. *Acta Crystallogr. D Biol. Crystallogr.* **66**, 213–221 [CrossRef Medline](#)
32. Murshudov, G. N., Vagin, A. A., and Dodson, E. J. (1997) Refinement of macromolecular structures by the maximum-likelihood method. *Acta Crystallogr. D Biol. Crystallogr.* **53**, 240–255 [CrossRef Medline](#)
33. Winn, M. D., Ballard, C. C., Cowtan, K. D., Dodson, E. J., Emsley, P., Evans, P. R., Keegan, R. M., Krissinel, E. B., Leslie, A. G., McCoy, A., McNicholas, S. J., Murshudov, G. N., Pannu, N. S., Potterton, E. A., Powell, H. R., et al. (2011) Overview of the CCP4 suite and current developments. *Acta Crystallogr. D Biol. Crystallogr.* **67**, 235–242 [CrossRef Medline](#)
34. Wyatt, P. J. (1993) Light scattering and the absolute characterization of macromolecules. *Anal. Chim. Acta* **272**, 1–40 [CrossRef](#)
35. Schuck, P. (2000) Size-distribution analysis of macromolecules by sedimentation velocity ultracentrifugation and Lamm equation modeling. *Biophys. J.* **78**, 1606–1619 [CrossRef Medline](#)
36. Hess, B., Kutzner, C., van der Spoel, D., and Lindahl, E. (2008) GROMACS 4: Algorithms for highly efficient, load-balanced, and scalable molecular simulation. *J. Chem. Theory Comput.* **4**, 435–447 [CrossRef Medline](#)
37. Schmid, N., Eichenberger, A. P., Choutko, A., Riniker, S., Winger, M., Mark, A. E., and van Gunsteren, W. F. (2011) Definition and testing of the GROMOS force-field versions 54A7 and 54B7. *Eur. Biophys. J.* **40**, 843–856 [CrossRef Medline](#)
38. Malde, A. K., Zuo, L., Breeze, M., Stroet, M., Poger, D., Nair, P. C., Oostenbrink, C., and Mark, A. E. (2011) An automated force field topology builder (ATB) and repository: Version 1.0. *J. Chem. Theory Comput.* **7**, 4026–4037 [CrossRef Medline](#)
39. Darden, T., York, D. and Pedersen, L. (1993) Particle mesh Ewald: An N-log(N) method for Ewald sums in large systems. *J. Chem. Phys.* **98**, 10089–10092 [CrossRef](#)
40. Bussi, G., Donadio, D., and Parrinello, M. (2007) Canonical sampling through velocity rescaling. *J. Chem. Phys.* **126**, 014101 [Medline](#)